Cyclic Ozone Identified in Magnesium Oxide (111) Surface Reconstructions

Richard Plass,[1] Kenneth Egan,[1] Chris Collazo-Davila,[2] Daniel Grozea,[2] Eric Landree,[2]
Laurence D. Marks,[2] and Marija Gajdardziska-Josifovska[1]
[1]*Department of Physics, University of Wisconsin-Milwaukee, Milwaukee, Wisconsin 53201*
[2]*Department of Materials Science and Engineering, Northwestern University, Evanston, Illinois 60208*
(Received 9 December 1997)

We report the first experimental evidence of the cyclic form of ozone, found in three air stable surface reconstructions of MgO (111) annealed above 1450 °C. The MgO (111)-$(\sqrt{3} \times \sqrt{3})R30°$ surface consists of equilateral oxygen trimers while the MgO (111)-(2×2) and MgO (111)-$(2\sqrt{3} \times 2\sqrt{3})R30°$ surfaces are periodic arrangements of trimers and single oxygen atoms. The oxygen trimers appear to be centered over underlying Mg atoms. The structures fit transmission electron diffraction data better than neutral plane faceting based models proposed for the polar MgO (111) surface. [S0031-9007(98)07807-7]

PACS numbers: 61.14.Rq, 61.16.Bg, 68.35.Bs

The stability of polar oxide surfaces has long been a problematic question in surface science. A bulk terminated polar surface has an infinite surface energy because alternating layers of oppositely charged ions produce a large dipole moment perpendicular to the surface [1]. For the model MgO (111) polar oxide surface theoretical results have pointed to two similar solutions for this problem: microscopic faceting into neutral {100} planes upon annealing [2–5] and surface reconstructions, which are essentially faceting to neutral planes but on an atomic scale [5–7].

The microscopic faceting model has long been supported by low energy electron diffraction (LEED) and scanning electron microscopy (SEM) of 1200 °C annealed MgO (111) surfaces [8,9] which revealed micron-sized triangular facets. These facets were interpreted to be neutral {100} planes. It has been recently shown, however, that these facets are much shallower vicinal {111} planes introduced by acid etching in sample preparation [10]. Upon higher temperature annealing these vicinal planes "heal" to an MgO (111) surface with large terraces and step bunches [10].

Reflection high energy electron diffraction (RHEED) experiments identified an air stable $(\sqrt{3} \times \sqrt{3})R30°$ reconstruction on these terraces and reflection electron energy loss spectroscopy (REELS) determined that the reconstructed surface was oxygen rich [11]. Theoretical studies have proposed four surface reconstructions for MgO (111): $(\sqrt{3} \times \sqrt{3})R30°$ (or just $\sqrt{3}$ hereafter, 5.15 Å unit cell) [6], a related $(2\sqrt{3} \times 2\sqrt{3})R30°$ ($2\sqrt{3}$ hereafter, 10.3 Å unit cell) [6], 2×1 [5], and 2×2 (5.95 Å unit cell) [5,7]. These reconstruction models all remove atoms periodically from the bulk terminated MgO (111) surface, generating atomic scale facets of neutral surfaces. We report here, however, that based on transmission electron diffraction (TED) data, the key features of the $\sqrt{3}$, 2×2, and $2\sqrt{3}$ reconstructions are equilateral trimers of oxygen or cyclic ozone. To the best of our knowledge, this is the first experimental evidence for the conjectured isomer of atmospheric ozone [12–18].

Single crystal MgO samples with (111) surfaces were prepared for the TED studies on 3 mm diameter, 150 μm thick disks which were mechanically dimpled, polished, and Ar^+ ion milled to electron transparency in the center. The samples were then annealed in an MgO lined tungsten boat vacuum furnace to between 1450 and 1650 °C (as measured by an optical pyrometer) for 30 min to 4.5 h and at a typical pressure of 5×10^{-7} Torr (see Ref. [10] for more details). Subsequent *ex situ* TED studies were done at 300 kV in a Hitachi H-9000 NAR transmission electron microscope. The three observed surface reconstructions, shown in Figs. 1(a)–1(c), appear in the order $\sqrt{3}$, 2×2, and $2\sqrt{3}$ with increasing annealing temperature. To minimize dynamical diffraction effects (which complicate subsequent data analysis), the reconstructions' diffraction patterns were recorded 40 to 90 mrad away from the [111] zone orientation [19]. Through exposure TED patterns were recorded for each reconstruction from different sample regions with thicknesses ranging from 250 to 425 Å. The exposure series were digitized with a microdensitometer, and beam intensities and errors were obtained using a cross correlation technique [20]. Symmetrical, weighted averaging was then done to yield different final data sets in which $p3$, $p3m1$, and $p31m$ symmetries were imposed. For $p3m1$ symmetry this yielded two data sets (5 and 6 unique beams) for $\sqrt{3}$, one data set (9 beams) for 2×2, and two data sets (39 and 37 beams) for $2\sqrt{3}$. The strongest relative beam intensities and errors for $p3m1$ symmetry are listed in Table I.

If the phases of these diffracted beams are known, a reverse Fourier transform directly maps the scattering potential and hence the projected atomic locations. Generally these phases are unknown, but for a given periodicity and symmetry, atomic scattering puts restrictions on the phases which are possible (e.g., [21,22]). Direct methods are numerical procedures which find phase sets for the intensity data which are consistent with these restrictions (e.g., [21–29]). Reference [22] provides a detailed explanation of the specific and rather involved numerical

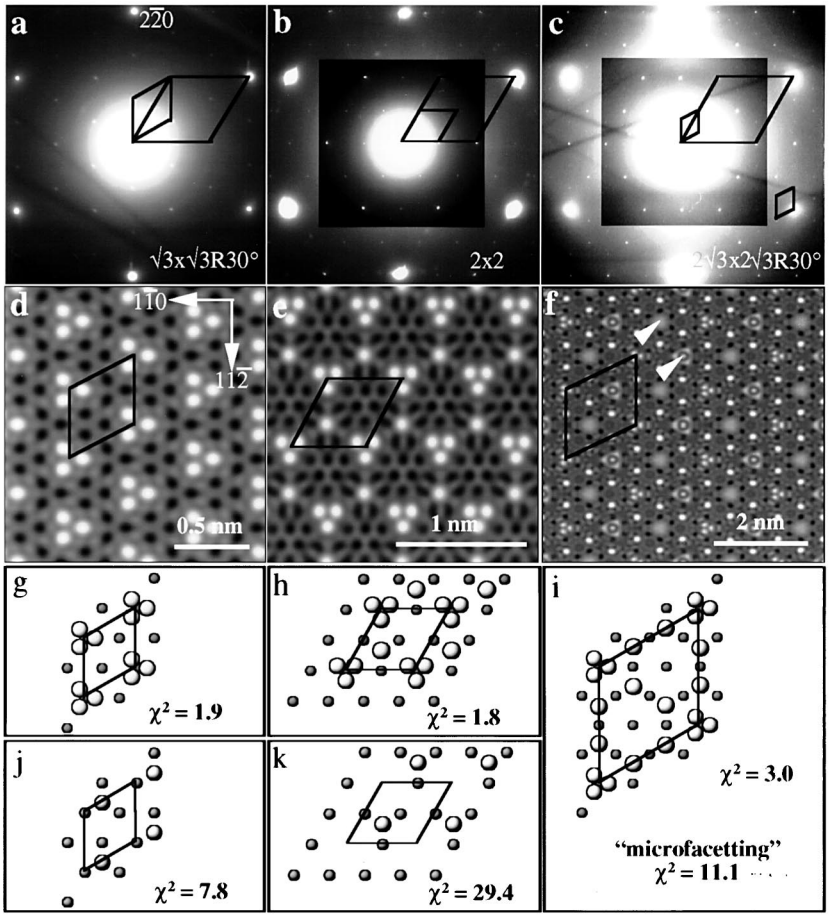

FIG. 1. Transmission electron diffraction patterns of (a) MgO (111)-($\sqrt{3} \times \sqrt{3}$)$R30°$ (or just $\sqrt{3}$, as in the text), (b) MgO (111)-(2×2) (just 2×2), and (c) MgO (111)-($2\sqrt{3} \times 2\sqrt{3}$)$R30°$ (just $2\sqrt{3}$) with reconstructed unit cells (smaller rhombuses) and MgO (111)-(1×1) unit cells (larger rhombuses) shown. Direct method maps for (d) $\sqrt{3}$, (e) 2×2, and (f) $2\sqrt{3}$ all show bright equilateral trimer features and additional single features in (e) 2×2, and (f) $2\sqrt{3}$. Simulations show these trimer features are periodic arrays of cyclic ozone molecules and the single features are lone oxygen atoms. (g),(i) are top view schematic diagrams of the cyclic ozone starting models for the (g) $\sqrt{3}$, (h) 2×2, and (i) $2\sqrt{3}$ surface structures along with denoted χ^2 values of atomic position refined kinematical models which allow trimer rotation. These χ^2 values are much lower than the χ^2 values of the (j) "microfaceting" $\sqrt{3}$ model [6], and (k) the "octopolar" 2×2 model [5,7]. The "microfaceting" based $2\sqrt{3}$ model is not shown here though its χ^2 value is listed in (i). The surface unit cells are shown in (d) through (k) and in (g) through (k) the large light balls are surface O atoms, while the small dark balls are second layer Mg atoms.

procedure used. Once obtained, the phase sets, and their corresponding real space maps, are ranked by a figure of merit which measures how well each phase set/map matches atomic scattering potentials. The maps with the best figures of merit are good starting points for atom position refinement algorithms [22].

Shown in Figs. 1(d)–1(f) are typical maps for the three reconstruction periodicities upon which $p3m1$ symmetry has been imposed; bright features correspond to likely projected positions of surface atoms. Most of the solutions for the $p3$ and $p3m1$ symmetries had essentially the same features as those seen in Figs. 1(d)–1(f); $p31m$ solutions predicted very unrealistic atomic sites. From these solutions Fourier subtraction techniques were used to check for other possible atomic sites, but none were found. At this point the measurement errors of the intensities were included in the data sets. Kinematical (single scattering) χ^2 refinements of the atomic starting models were then performed. These refinements allow comparison of our models and literature models to the experimental TED data and are also a first step towards more involved dynamical (multiple scattering) χ^2 refinements.

As is shown in Fig. 1(d), the $\sqrt{3}$ map has a regular pattern of bright trimer features with roughly 1.5 Å spacings. These trimers also appear in the 2×2 and $2\sqrt{3}$ maps, Figs. 1(e) and 1(f), respectively, along with single bright features. If oxygen atoms are assigned to all the bright feature locations in the maps, then simulated diffraction patterns calculated from the resulting reconstruction models consistently fitted the experimental data better than assignment of Mg atoms or a mixture of Mg and O. Therefore, the trimers seen in the maps are cyclic ozone molecules bonded to the MgO surface. Assignment of possible foreign atomic species such as W, Si, Ca, and C also fitted the data poorly, in agreement with *in situ* x-ray photoelectron spectroscopy (XPS) of a $\sqrt{3}$ sample which showed only

TABLE I. Strongest $p3m1$ symmetrized surface beam intensities and errors relative to the most intense surface beam obtained from experimental TED patterns of the MgO (111)-$(\sqrt{3} \times \sqrt{3})R30°$, MgO (111)-$(2 \times 2)$, and MgO (111)-$(2\sqrt{3} \times 2\sqrt{3})R30°$ surface reconstructions.

			Set #1		Set #2	
Reconst.	Index		Intensity	Error	Intensity	Error
$\sqrt{3}$	1	0	1.000	0.146	1.000	0.130
	2	0	0.243	0.049	0.144	0.023
	2	1	0.139	0.056	0.093	0.023
	4	0	0.110	0.018	0.067	0.014
	3	1	0.126	0.045	0.070	0.022
2×2	1	0	1.000	0.244		
	1	1	0.668	0.041		
	3	0	0.149	0.027		
	2	1	0.143	0.038		
	3	1	0.106	0.028		
	3	2	0.100	0.023		
$2\sqrt{3}$	3	0	1.000	0.112	1.000	0.101
	4	0	0.015	0.011	0.021	0.005
	3	1	0.042	0.015	0.058	0.017
	5	0	0.019	0.002	0.014	0.010
	5	1	0.035	0.008	0.039	0.009
	4	2	0.018	0.003	0.021	0.006
	3	3	0.310	0.039	0.257	0.051
	9	0	0.055	0.020	0.048	0.009
	6	3	0.101	0.018	0.069	0.019

strong Mg and O peaks [10]. (A small carbon peak, presumably from air transport CO_2 contamination, was seen in an *ex situ* XPS analysis of a $\sqrt{3}$ TED sample.) Mg or O atoms included at the less bright locations in Fig. 1(f) (at arrows) worsened the fit to the experimental data. These features are likely artifacts due to incomplete data (i.e., bulk and surface termination beams must be excluded), as are the dark features in Figs. 1(d)–1(f) [22,23].

The $\sqrt{3}$ and $2\sqrt{3}$ maps have the oxygen trimer sides aligned with the $\langle 211 \rangle$ directions, meaning that they are angled 30° out of alignment with the underlying bulk atom positions. In contrast, the trimer sides of 2×2 are aligned with the $\langle 110 \rangle$ directions. Kinematical χ^2 refinements confirm the $\sqrt{3}$ $\langle 211 \rangle$ alignment (total χ^2 of 1.9 for both data sets and an oxygen to oxygen trimer spacing of 1.53 Å) but favor an approximate 15° rotation angle from the $\langle 110 \rangle$ direction for 2×2 (χ^2 of 1.8 for a trimer spacing of 1.55 Å) and again 15° but from the $\langle 211 \rangle$ type direction for $2\sqrt{3}$ (total χ^2 of 3.0 for both data sets and a trimer spacing of 1.26 Å). These results strongly suggest that the cyclic ozone molecule can pivot about its center, although the symmetrization of off-zone TED data and the relative simplicity of the kinematical models call the exact rotation angles (and trimer spacings) into some question.

Neither the direct method maps nor the kinematical χ^2 analysis provide information on surface registry to the bulk crystal. However, in the $2\sqrt{3}$ map, Fig. 1(f), we see a honeycomb of oxygen atoms in addition to the oxygen trimers. This honeycomb sets the most likely registry since, as seen from the stacking fault calculations of Wolf [7], having an O atom directly over an Mg atom on a (111) type surface is energetically unfavorable. There is then only one surface registry for the $2\sqrt{3}$ oxygen honeycomb which avoids this configuration, which is shown in the model in Fig. 1(i). Besides placing half of the honeycomb oxygen atoms in stacking fault type sites, this constraint positions the center of the $2\sqrt{3}$ cyclic ozone trimer directly over an Mg atom one layer down. This configuration agrees very well with a clearly established coordination chemistry principle which states that a cation will always prefer to sit in the center of a π-bonded ring ligand, as is seen, for example, in the structure of magnesium cyclopentadienyl, $Mg(C_5H_5)_2$. It also agrees with cyclic ozone's apparent ability to pivot about its center: the underlying Mg atom is the pivot point. Hence, we assume the same registry between cyclic ozone and Mg atoms in the $\sqrt{3}$ and 2×2 model structures, as is shown in Figs. 1(g) and 1(h) [30]. Unfortunately, one critical datum, the vertical spacing of cyclic ozone over the second Mg layer, cannot be obtained from two-dimensional TED data.

To compare our cyclic ozone models to existing faceting based atomic models, the latter were also simulated. The "microfaceting" $\sqrt{3}$ model of Watson *et al.* [6] and the "octupole" 2×2 model of Wolf [7] and Pojani *et al.* [5] are shown in Figs. 1(j) and 1(k) (see Ref. [6] for an illustration of the deeper, four-layer, "microfaceting" $2\sqrt{3}$ model). In all cases the cyclic ozone models yielded substantially better χ^2 fits to the experimental TED data, as listed in Figs. 1(g)–1(k).

Confirmation of the existence of cyclic ozone ties into the long-standing chemistry question of which isomer of ozone is most stable and why. The bent structure of atmospheric ozone (116.8° bend angle and 1.27 Å bond distance) is well established [31,32], but initially ozone was conjectured to have an equilateral triangle shape, an assumption which gained theoretical support from the molecular orbital calculations of Peyerimhoff and Buenker [12]. Since then the differences between neutral bent and cyclic ozone have been extensively studied with focus on cyclic ozone's possible role in atmospheric chemistry (e.g., [13–18] and references therein). The angular potential curves of Shih *et al.* [13] and the potential energy surface crossing points between bent and cyclic ozone of Xantheas *et al.* [33] suggest that if ozone starts forming with a bend angle below 84°, then the resulting 60° configuration is metastable with respect to the bent form, but a formation mechanism is lacking. While neutral cyclic ozone has not been observed, there are indications that a charged form of cyclic ozone may exist. Peyerimhoff and Buenker [12] pointed out that if one were to add more molecular electrons to a triatomic molecule (whose atoms have similar electronegativities) then a smaller molecule bend angle would result. This trend is confirmed experimentally, for instance, in the 110° bend angle of the ozonide ion, O_3^- [34,35]. Thus charge transfer from one or more second

layer Mg atoms may have a major role in forming and stabilizing cyclic ozone. Charge transfer can also explain the stabilization of the polar MgO (111) surface [5] and ionic ligand bonding can explain the MgO (111) reconstructed surfaces' unexpected air stability.

To investigate possible charge transfer within the kinematic cyclic ozone models, atomic scattering factors for neutral Mg, neutral O, Mg^{+1}, Mg^{+2}, O^{-1}, and O^{-2}, were tested in the refinements (± 1 scattering factors were interpolated from the neutral [36] and ± 2 [37] scattering factors). However, the resulting kinematical χ^2 values showed only slight variations with charge, favoring the ± 1 states. Despite charge affecting only the lowest order beams, dynamical χ^2 refinements may be more sensitive to this key parameter. Full dynamical χ^2 refinements are in progress to determine more precisely the oxygen to oxygen spacing, the mean trimer rotation angle (and possible distribution), the charge on the surface and subsurface species, the subsurface relaxations, the effect of both surfaces being reconstructed [38,39], and the presence of a complete second layer of Mg atoms. The spacing of cyclic ozone above the central Mg atom will have to be determined by another technique. Theoretical treatment of charged species of cyclic ozone is also needed as are experimental studies of the reactivity and catalytic properties of ozone stabilized MgO (111) surfaces. Infrared spectroscopy of the reconstructed surfaces would be invaluable in confirming the presence of predicted cyclic ozone spectral absorptions [15,17,18].

To summarize, the theoretically predicted, atomic scale faceting based models fit our TED MgO (111) $(\sqrt{3} \times \sqrt{3})R30°$, (2×2), and $(2\sqrt{3} \times 2\sqrt{3})R30°$ surface reconstruction data very poorly. Much better agreement is obtained for models containing periodic arrays of equilateral trimers of oxygen, about 1.5 Å apart, i.e., cyclic ozone. Single oxygen atoms are also features of the (2×2), and $(2\sqrt{3} \times 2\sqrt{3})R30°$ reconstructed surfaces. That the cyclic ozone molecules are likely centered over Mg ions one layer down is concluded from surface registry and ionic ligand chemistry arguments.

We thank W. England, D. Wolf, and J. M. Zuo for their most fruitful discussions and correspondence. This work was supported by the National Science Foundation at UWM under a Presidential Faculty Fellowship Award, Grant No. NSF/DMR-9553148, and at NU under NSF/DMR-9705081.

[1] F. Bertaut, Comput. Rendu. **246**, 3447 (1958).
[2] P. W. Tasker, J. Phys. C **12**, 4977 (1979).
[3] P. A. Cox, F. W. H. Dean, and A. A. Williams, Vacuum **33**, 839 (1983).
[4] A. Gibson, R. Haydock, and J. P. LaFemina, J. Vac. Sci. Technol. A **10**, 2361 (1992).
[5] A. Pojani *et al.*, Surf. Sci. **387**, 354 (1997).
[6] G. W. Watson *et al.*, J. Chem. Soc. Faraday Trans. 2 **92**, 433 (1996).
[7] D. Wolf, Solid State Ionics **75**, 3 (1995); Phys. Rev. Lett. **68**, 3315 (1992).
[8] V. E. Henrich, Surf. Sci. **57**, 385 (1976).
[9] H. Onishi *et al.*, Surf. Sci. **191**, 479 (1987).
[10] R. Plass, J. Feller, and M. Gajdardziska-Josifovska, Surf. Sci. **414**, 26 (1998).
[11] M. Gajdardziska-Josifovska, P. A. Crozier, and J. M. Cowley, Surf. Sci. Lett. **248**, L259 (1991); P. A. Crozier, M. Gajdardziska-Josifovska, and J. M. Cowley, Microsc. Res. Tech. **20**, 426 (1992).
[12] S. D. Peyerimhoff and R. J. Buenker, J. Chem. Phys. **47**, 1953 (1967).
[13] S. Shih, R. J. Buenker, and S. D. Peyerimhoff, Chem. Phys. Lett. **28**, 463 (1974).
[14] J. S. Wright, Can. J. Chem. **51**, 139 (1973).
[15] P. J. Hay and T. H. Dunning, J. Chem. Phys. **67**, 2290 (1977).
[16] P. G. Burton, J. Chem. Phys. **71**, 961 (1979).
[17] T. J. Lee, Chem. Phys. Lett. **169**, 529 (1990).
[18] A. S. Shalabi, J. Mol. Struct. **262**, 131 (1992).
[19] P. Xu and L. D. Marks, Ultramicroscopy **45**, 155 (1992).
[20] P. Xu, G. Jayaram, and L. D. Marks, Ultramicroscopy **53**, 15 (1994).
[21] M. M. Woolfson, Acta Crystallogr. Sect. A **43**, 593 (1988).
[22] L. D. Marks *et al.*, Surf. Rev. Lett. **5**, 1087 (1998).
[23] L. D. Marks, R. Plass, and D. Dorset, Surf. Rev. Lett. **4**, 1 (1997).
[24] C. J. Gilmore *et al.*, Surf. Sci. **381**, 77 (1997).
[25] C. Collazo-Davila, D. Grozea, and L. D. Marks, Phys. Rev. Lett. **80**, 1678 (1998).
[26] E. Landree, C. Collazo-Davila, and L. D. Marks, Acta Crystallogr. Sect. B **53**, 916 (1997).
[27] L. D. Marks and E. Landree, Acta Crystallogr. Sect. A **54**, 296 (1998).
[28] D. Sayre, Acta Crystallogr. **5**, 60 (1952).
[29] J. Karle and H. Hauptman, Acta Crystallogr. **9**, 635 (1956).
[30] The kinematical χ^2 refinements were not conclusive about the occupancy of the underlying layer of Mg atoms. In two cases having a single Mg atom per unit cell at the center of the trimer produced a better χ^2 than a full second layer of Mg atoms: $\chi^2 = 1.8$ for a single Mg atom vs 3.4 for the full Mg layer in 2×2 and $\chi^2 = 3.0$ for a single atom vs 3.9 for the full layer in $2\sqrt{3}$. However, $\sqrt{3}$ was somewhat better fitted with a full layer of Mg atoms: $\chi^2 = 1.9$ for the full layer vs 2.2 for a single atom.
[31] R. J. Hughes, Chem. Phys. **24**, 131 (1956).
[32] P. J. Durrant and B. Durrant, *Introduction to Advanced Inorganic Chemistry* (Wiley, New York, 1962), p. 799.
[33] S. Xantheas, S. T. Elbert, and K. Ruedenberg, J. Chem. Phys. **93**, 7519 (1990).
[34] I. I. Vol'nov, *Peroxides, Superoxides and Ozonides of Alkali and Alkaline Earth Metals* (Plenum, New York, 1966), p. 125.
[35] L. Andrews, J. Chem. Phys. **63**, 4465 (1975).
[36] P. A. Doyle and P. S. Turner, Acta Crystallogr. Sect. A **24**, 390 (1968).
[37] L. M. Peng, Acta Crystallogr. Sect. A **54**, 481 (1998); J. M. Zuo (private communication).
[38] L. M. Peng and M. J. Whelan, Acta Crystallogr. Sect. A **47**, 101 (1991).
[39] L. D. Marks, Ultramicroscopy **45**, 145 (1992).